Magnetochemistry

Additive Manufacturing of Cobalt-Based Organic Ferromagnetic Materials

Junfeng Huang[1], Kam Chuen Yung[1], Zhengong Meng[2], Desmond T. C. Ang[1], and Guijun Li[1]

[1]*Department of Industrial and Systems Engineering, The Hong Kong Polytechnic University, Hung Hom, Hong Kong*
[2]*Department of Chemistry, Hong Kong Baptist University, Kowloon, Hong Kong*

Received 3 Jan 2017, revised 25 Jan 2017, accepted 25 Jan 2017, published 31 Jan 2017, current version 22 Mar 2017.

Abstract— Clogging problems from the aggregation of dispersed solutes have hindered the successful application of inkjet printing for patterning ferromagnetic materials. Native ferromagnetic ink with complete solubility and proper surface tension for inkjet printing has been lacking. Here, we report a metal-organic molecule with absolute solubility in dimethylformamide (DMF) solvent, which can be successfully patterned using state-of-art inkjet printing technologies. The jetting parameters for this ferromagnetic ink were systemically optimized and a series of patterns were successfully made on a variety of substrates. These patterned ferromagnetic 2.5-dimensional structures showed ferromagnetic properties as experimentally verified.

Index Terms—Magnetochemistry, additive manufacturing, metal-organic, 2.5-dimensional structures.

I. INTRODUCTION

Inkjet printing of magnetic materials with three-dimensional (3D) structures has attracted wide attention in recent years [Li 2014, Wu 2010]. Due to its low cost and ambient processing features, inkjet printing is one of the most attractive additive manufacturing methods for fabricating flexible and miniaturized 3D microdevices [Sirringhaus 2000, de Gans 2004, Kang 2010, 2012, Lee 2010]. Nanoparticle ink was successfully adopted in drop-on-demand inkjet printing, and various applications were achieved via this economical plus easy-to-operate technique. However, it still suffers from clogging problems with materials agglomeration during printing [Yung 2009]. Dispersion ink tends to aggregate due to its insolubility and the dynamic viscosity changes as time passes and temperature increases, causing materials to aggregate and subsequently clog the nozzle. To address these challenges, metal-organic ink was developed to enhance stability and dispersity by reducing the particle–particle interaction, thereby decreasing the aggregation risk [Jahn 2008, Elgammal 2016]. Metal-organic ink contains dissolved molecules which are completely dissolved into solution rather than in suspension. Such ink does not undergo sedimentation in the inkjet nozzle, thereby improving printability. In addition, synthesized chemical precursors should possess solubility in regular solvents, excellent adhesion to various substrates, and uniformity as multilayer films [Mei 2005]. Surface tension of the inks should be between 30∼70 mN/m, which should be sufficient to remain in the nozzle without dripping and spread over the substrate surface to form continuous films [Yun 2009]. At the same time, the coffee-ring effect would influence the accuracy of the desired patterns [Wu 2015]. Therefore, it is important to optimize the distance between each droplet. Determining the optimized spacing length between each droplet has been widely studied [Stringer 2009, 2010]. Substrate properties, solution adhesion and other parameters are critical factors in the determination of the droplet space.

Corresponding author: G. Li (mitch.li@polyu.edu.hk). International Conference of the Asian Union of Magnetics Societies, Tainan, Taiwan, 1-5 August 2016.
Digital Object Identifier 10.1109/LMAG.2017.2661720

Promising magnetic materials and relative applications formed by inkjet printing have been comprehensively studied. As soft magnetic material, NiZn-ferrite was developed to form the integration of radio-frequency passive components with inkjet printing [Bissannagari 2015]; a microelectromechanical system component was built with superparamagnetic SU-8 [Jacot-Descombes 2014]; ferromagnetic materials were also used to fabricate various types of microscale devices by inkjet printing technology [Lee 2013]. Besides, magnetic materials built by this additive manufacturing for numerous applications in wide fields have been reported, such as the radio-frequency identification resonators [Marjanovic 2014], and electromagnetically driven actuators that generated magnetic fields to stimulate the beam [Ando 2016]. In biomedical applications, photonic crystal microchips for detection of fluorescence analytes [Hou 2014] and circulating tumor cells with sufficient magnetic force [Chen 2016] were also obtained in this non-contact and mask-less printing technology. Ferromagnetic ring structure, also defined as ring-shape ferromagnetic elements, contributed to manifold potential applications, including cell culture arrays for biomedical research [Huang 2015], diluted magnetic semiconductors [Nkosi 2013], and domain-wall conduits [Donolato 2010].

As one of the most important transition metals with ferromagnetic properties, cobalt-based materials have aroused much interest in structuring magnetic components. Cobalt-based thin films based on inkjet printing have been comprehensively studied [Lee 2013, Fittschen 2006, Shen 2006]. Thus, the development of 3D structural thin film magnetic components for cobalt-organic molecular nanoparticles in inkjet printing technology has become a priority. Unfortunately, there is no report on inkjet printing of fully dispersed cobalt-based ferromagnetic ink to our knowledge.

Here, we report an additive manufacturing method for constructing 2.5-dimensional (2.5D) structure multilayer patterns with ferromagnetic properties. To solve the material agglomeration problem, synthesized cobalt-based molecular materials and a low volatility organic solvent was combined as metal-organic ink during inkjet printing. Revealed by vibrating sample magnetometer (VSM), scanning electron microscope (SEM), atomic force microscopy (AFM), magnetic

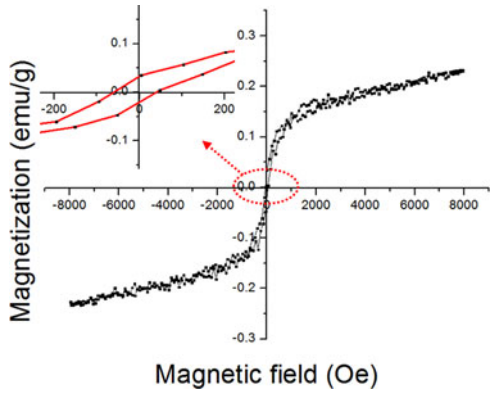

Fig. 1. Magnetization loop at room temperature for cobalt-based organic compound, $H_c = 50$ Oe.

force microscopy (MFM) and optical surface profiler, the microstructures, magnetic properties, and the optimum parameters of printed patterns were systemically studied.

II. MATERIALS

Cobalt-based organic material was synthesized via chemical methods [Mann 2011] and identified as $Co(tpy)Cl_2 \cdot MeCN$ in formula. The ferromagnetic properties of this material were characterized by VSM at room temperature as shown in Fig. 1. The result shows that the particles behave ferromagnetically with magnetic moments at 0.24 emu/g. The coercivity is approximately 50 Oe as shown in the inset image of Fig. 1.

III. EXPERIMENT

The 0.5 mmol $Co(tpy)Cl_2 \cdot MeCN$ was dissolved into 1.5 ml dimethylformamide (DMF). After sonication for 30 minutes, the mixture solution was filtered with a syringe filter (0.22 μm). Two types of substrates, glass slides and silicon wafers, were cleaned with sonication in acetone, water, and methanol in sequence. An inkjet printing head (model Microdrop MD-K-130) with nozzle diameter at 30 μm was used after mounting on a homemade *X-Y* moving stage with CAD controls [Yung 2016]. The distance from the nozzle to the substrate was fixed at 0.4 mm. The step spacing was 0.15 μm. Printing period and delay for the droplets were 9650 μs and 704 μs, respectively. The speed for the moving stage was fixed at 500 mm/min. During printing, the substrates were heated up to 100 °C with a hot plate.

IV. RESULTS AND ANALYSIS

A. Optimized Droplet Spacing on Different Substrates

Patterns generated by overlapping individual drops were demonstrated for studying the optimized dropping distance with glass slides as substrates. Fig. 2(a) shows the optical microscopy image of multi-line shape patterns with 80 μm droplet spacing. For comparison, the image of line shape pattern with 110 μm distance is examined in Fig. 2(b). As shown in Fig. 2(a) and (b), the diameter of the droplet on the substrate was approximately 240 μm on average. The pattern in Fig. 2(a) was printed in the direction as the label shown in the left

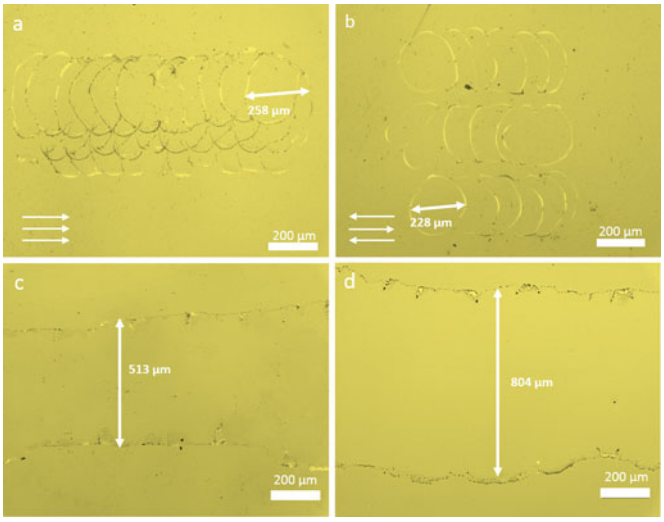

Fig. 2. (a) Optical microscopy image of multi-line shape pattern with 80 μm spacing distance. (b) Optical microscopy image of line shape pattern with 110 μm spacing distance. (c) Optical microscopy image of one-line pattern on the glass slide. (d) Optical microscopy image of one-line pattern on the silicon wafer.

corner and printed in different directions in Fig. 2(b). To distinguish the intersection for each drop, the distances for each line were varied in Fig. 2(a) and (b). The coffee-ring effect [Denneulin 2011] was significant, where crystal-like materials dispersed on the boundary with distinct marks left due to the solution drying. Cobalt-based nanoparticles primarily concentrated on the edge of each drop. The latter droplet overlapped the former droplet's circle shape and formed another circle shape with intersection. Since the distance for each line was smaller than the diameter of droplet, intensive intersections occurred. However, in comparison with the patterns in Fig. 2(b), over-intersection of droplets seriously influenced the accuracy of patterns where many partial-ring marks were generated. Furthermore, there was not any critical effect in different printing directions. In addition, compared to Fig. 2(a) and (b), due to the different droplet-spacing distances, the printed pattern on the left revealed more distinct boundary marks caused by solvent drying.

To investigate the substrate influence, the $Co(tpy)Cl_2 \cdot MeCN$ nanoparticles were inkjet printed onto glass and silicon wafers using identical parameters. The contact angles of the ink were measured to be 17.6° for glass and 16.2° for silicon wafer. According to the spreading ratio equation [Lim 2009a], the spreading ratio β was calculated as 2.576 for glass and 2.650 for silicon wafer. As revealed from the optical microscopy results in Fig. 2(c) and (d), the width of the printed pattern in line shape was around 513 μm on the glass slides and 804 μm on the silicon wafer. The printed pattern in Fig. 2(c) revealed higher contrast compared with that in Fig. 2(d). With identical surface cleaning, the glass substrate exhibited unavoidable darkness while the silicon wafer showed distinct brightness, which was due to poor polishing of the glass slide [Dusza 2005]. In addition, higher spreading ratio resulted in less evaporation time, so the printing contrast was enhanced significantly. The evaporation time is deduced from the time evolution of the contact angle and shows an exponential decaying behavior with increasing substrate temperature [Girard 2006]. When the substrate temperature is moderately high, the drying time

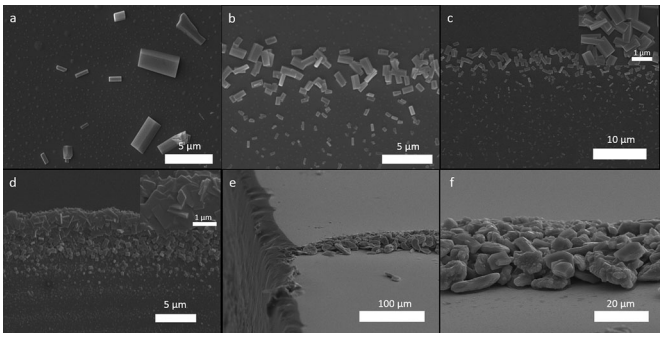

Fig. 3. (a) SEM image of particle on the glass slide. (b) SEM image of particle on the silicon wafer. (c) SEM image of one-line pattern at the edge in one-time printing. Inset is enlarged image. (d) SEM image of one-line pattern at the edge in ten-time printing. Inset is enlarged image. (e) SEM image of multi-line pattern in a 15° angle view in macroscopic aspect. (f) Magnified SEM image of multi-line pattern in a 15° angle view.

will be short enough to sustain growth of longer 3D structures. The ideal substrate temperature would be higher than the critical flocculation temperature [van den Berg 2007] but lower than the Leidenfrost temperature [Ko 2010]. Meanwhile, the reason evaporation leads to such a marked difference between the two substrates is the different thermal conductivity [Lim 2009b]. At the same time, the microstructures of the printed patterns were analyzed with SEM characterization. Fig. 3(a) and (b) present the printed patterns in the same condition on glass and on silicon wafer. Cuboid structures were observed on the substrate with typical length ranging from 300 nm to 3 μm at the long sides. Materials were distributed in ladder shape, decreasing from edge to center, which is consistent with the coffee-ring effects in Fig. 2. Accompanying crystallization, however, small spot-type marks were generated. These unexpected marks distributed more intensively and clearly in Fig. 3(a) than in Fig. 3(b). Lower spreading ratio and poor quality of surface resulted in these characters. It demonstrated that glass is not an appropriate substrate compared to silicon wafer. Thus, we used silicon wafer as the substrate for building the 2.5D printed pattern.

B. Microstructure of 2.5D Printed Patterns on Silicon Wafer

The SEM image of a straight-line pattern on silicon wafer after printing 10 times is shown in Fig. 3(d)]. For comparison, the image after one-time printing is presented in Fig. 3(c). As mentioned in Section IV-A, the Co(tpy)Cl_2· MeCN molecules were dispersed from boundary to center with a decreased profile, due to the coffee-ring effect where the concentration is low. In Fig. 3(c), these cuboid structures recrystallized near the edge incompactly, and the morphology of the magnified image inset exhibited mild aggregation. After printing 10 times, crystals were superimposed vertically to form 3D morphologies, shown in Fig. 3(d). The printed area was strewn with concentrated nanoparticles, and the edge part showed critical superimposition. In the enlarged image [inset in Fig. 3(d)], recrystallized nanoparticles mixed together and started to form irregular shapes resulting from substantial accumulation.

A 2.5D structural printed pattern was observed by SEM from macroscopic aspect in a 15° incident angle view, as shown in Fig. 3(e). A distinct line with certain height was constructed by Co(tpy)Cl_2 · MeCN with 200 times printing. The line type sample was generated with materials accumulation and crystal growth. Irregular crystal grew in rapid drying with heating to compose three-dimension microstructures. The magnified image for this area was shown in Fig. 3(f). Three-dimensional structures presented more explicitly and the height increased to approximately 10 μm. Large irregular crystals agglomerated vertically while apertures and holes were pitted in the sample.

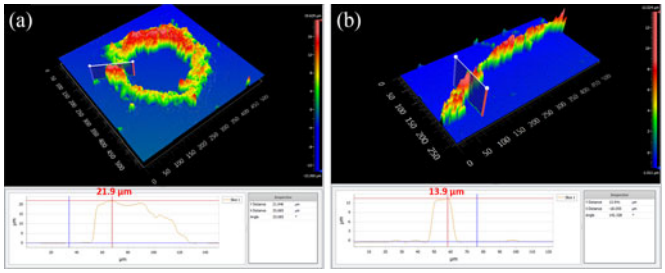

Fig. 4. (a) Optical surface profile image for multi-drop pattern. (b) Optical surface profile image for multi-line pattern.

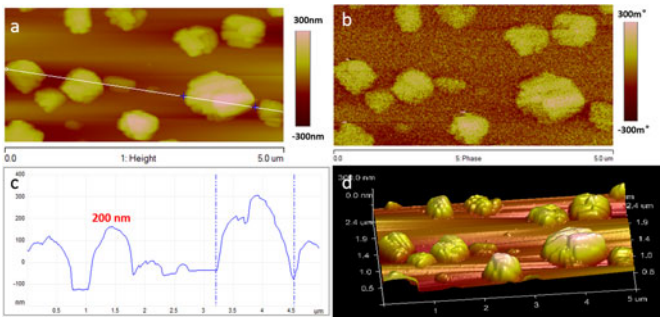

Fig. 5. (a) AFM image of the printed crystals. (b) Corresponding MFM image. (c) Corresponding AFM height profile. (d) 3D view of AFM image.

Optical surface profiler (Zygo Nexview) was used to obtain the 3D morphology of printed patterns. Fig. 4(a) presents the 2.5D structure of multi-drop pattern which was fabricated via 1000 times overlapping. The cross-section profile of the drop ring showed that the height of the Co(tpy)Cl_2 · MeCN was around 20 μm. It indicated that the repetitive printing could give rise to 2.5D structure building, which was consistent with the additive manufacturing mechanism. Similarly, the multi-line pattern also revealed 2.5D structures as shown in Fig. 4(b), where the sample was printed 100 times, and presented 12 μm height in cross-section. However, although these 2.5D structure could be built, the relationship between printing times and height was nonlinear. The 100-times printing can construct 12 μm height while 1000-times printing can only contribute 20 μm. Larger thickness required more droplet addition as the printed patterns grew. This nonlinear phenomenon was ascribed to the sample's lateral development. Accumulation in the horizontal direction severely affected vertical 2.5D structure building.

C. Characterization of Functional Magnetic Printing Ink

The morphology and magnetic topography of the nanoparticles after one-time printing was studied via AFM and MFM. Fig. 5(a) shows a topography image of cobalt-based ferromagnetic nanoparticles and Fig. 5(b) represent corresponding magnetic phase image. Magnetic

contrast appears in MFM phase image corresponding to the topographic bright and dark areas. The topography image shows the particles distributed with few overlapping. In this region, particles tended to form circle shapes. Agglomerated circle-shaped samples revealed extremely high brightness with almost 300 nm height. The subsequent MFM image [Fig. 5(b)] detected a distinct "magnetic contrast" at the same location. The magnetic contrast in the MFM image was almost consistent with the morphology in the corresponding AFM image, indicating the printed samples revealed strong magnetic signal and were proportionally accumulated with the amount of materials. In other words, the sample's topography and magnetic property were homogenous. The cross-section profile [white line in Fig. 5(a)] of the height information is shown in Fig. 5(c). The irregular profile demonstrated that the circle-shaped samples were aggregated by nanoparticles rather than single crystals, since they showed cuboid shapes in SEM images. The corresponding height profile showed that the average height of samples was approximately 200 nm. The relevant 3D view of the AFM image is shown in Fig. 5(d). Aggregated samples were presented on the surface spatially. From the images of height profile and 3D view, the patterns on the substrate should be identified as the accumulation of several particles rather than single particles. This demonstrated that the magnetic contrast was produced by multiparticles and it was consistent with the morphology signal in AFM.

D. Summary

From the above results, it can be clearly seen that the printing resolution plays an important role in inkjet printing. Printing droplet spacing and printing direction were investigated to reach optimum resolution. Because of its spreading ratio caused by the surface tension, the type of substrate was one of the determinative factors for optimum printing resolution. Due to low concentration of the ink, printed patterns suffered from the coffee-ring effect significantly, though increased substrate temperature might reduce this effect. As silicon wafer acted as the ideal substrate, 2.5D structural printed patterns were built. Cobalt-based materials were proportionally accumulated vertically with multiple printings. As shown in the magnetic property characterization, printed samples presented coherent magnetic signals as the $Co(tpy)Cl_2 \cdot MeCN$ crystals accumulated.

V. CONCLUSION

Ferromagnetic $Co(tpy)Cl_2 \cdot MeCN$ with complete solubility in DMF were synthesized and patterned with inkjet printing. The optimum droplet spacing for inkjet printing on silicon substrate was 110 μm. The 2.5D structured patterns were successfully built by inkjet printing on the silicon wafer as revealed by an optical surface profiler. Magnetic properties of $Co(tpy)Cl_2 \cdot MeCN$ after printing were characterized and they were consistent with relevant morphology. Other metal-organic inks with magnetic properties will be explored in the future.

ACKNOWLEDGMENT

This work was supported by the Hong Kong Polytechnic University under RUV2 Project.

REFERENCES

Andò B, Marletta V (2016), "An all-inkjet printed bending actuator with embedded sensing feature and an electromagnetic driving mechanism," *Actuators*, vol. 5, 21, doi: 10.3390/act5030021.

Bissannagari M, Kim J (2015), "Inkjet printing of NiZn-ferrite films and their magnetic properties," *Ceram. Int.*, vol. 41, pp. 8023–8027, doi: 10.1016/j.ceramint.2015.02.151.

Chen P, Huang Y-Y, Bhave G, Hoshino K, Zhang X (2016), "Inkjet-print micromagnet array on glass slides for immunomagnetic enrichment of circulating tumor cells," *Ann. Biomed. Eng.*, vol. 44, pp. 1710–1720, doi: 10.1007/s10439-015-1427-z.

de Gans B-J, Duineveld P C, Schubert U S (2004), "Inkjet printing of polymers: State of the art and future developments," *Adv. Mater.*, vol. 16, pp. 203–213, doi: 10.1002/adma.200300385.

Denneulin A, Bras J, Carcone F, Neuman C, Blayo A (2011), "Impact of ink formulation on carbon nanotube network organization within inkjet printed conductive films," *Carbon*, vol. 49, pp. 2603–2614, doi: 10.1016/j.carbon.2011.02.012.

Donolato M, Vavassori P, Gobbi M, Deryabina M, Hansen M F, Metlushko V, Ilic B, Cantoni M, Petti D, Bertacco R (2010), "On-chip manipulation of protein-coated magnetic beads via domain-wall conduits," *Adv. Mater.*, vol. 22, pp. 2706–2710, doi: 10.1002/adma.201000146.

Dusza J, Danzer R, Morrell R (2005), "Scratchability of soda-lime silica (SLS) glasses: Dynamic fracture analysis," *Key Eng. Mater.*, vol. 290, pp. 31–38, doi: 10.4028/www.scientific.net/KEM.290.31.

Elgammal M, Schneider R, Gradzielski M (2016), "Development of self-curable hybrid pigment inks by miniemulsion polymerization for inkjet printing of cotton fabrics," *Dyes Pigments*, vol. 133, pp. 467–478, doi: 10.1016/j.dyepig.2016.06.033.

Fittschen U E A, Hauschild S, Amberger M A, Lammel G, Streli C, Förster S, Wobrauschek P, Jokubonis C, Pepponi G, Falkenberg G, Broekaert J A C (2006), "A new technique for the deposition of standard solutions in total reflection X-ray fluorescence spectrometry (TXRF) using pico-droplets generated by inkjet printers and its applicability for aerosol analysis with SR-TXRF," *Spectrochim. Acta B: Atom. Spectr.*, vol. 61, pp. 1098–1104, doi: 10.1016/j.sab.2006.09.009.

Girard F, Antoni F, Faure S, Steinchen A (2006), "Evaporation and Marangoni driven convection in small heated water droplets," *Langmuir*, vol. 22, pp. 11085–11091, doi: 10.1021/la0615721.

Hou J, Zhang H, Yang Q, Li M, Song Y, Jiang L (2014), "Bio-inspired photonic-crystal microchip for fluorescent ultratrace detection," *Angew. Chem. Int. Edit.*, vol. 53, pp. 5791–5795, doi: 10.1002/anie.201400686.

Huang C-Y, Lai M-F, Ger T-R, Wei Z-H (2015), "Cell culture arrays using micron-sized ferromagnetic ring-shaped thin films," *J. Appl. Phys.*, vol. 117, 17B309, doi: 10.1063/1.4913816.

Jacot-Descombes L, Gullo M R, Cadarso V J, Mastrangeli M, Ergeneman O, Peters C, Fatio P, Freidy M A, Hierold C, Nelson B J, Brugger J (2014), "Inkjet printing of high aspect ratio superparamagnetic SU-8 microstructures with preferential magnetic directions," *Micromachines*, vol. 5, pp. 583–593, doi: 10.3390/mi5030583.

Jahn S F, Jakob A, Reinhold I, Engisch L, Lang H, Baumann R R (2008), "Structuring of flexible substrates by the use of an aqueous solution based silver ink," in *24th Int. Conf. Digital Printing Technologies, Tech. and Digital Fabrication Program Proc.*, pp. 684–688 [Online]. Available: http://publica.fraunhofer.de/documents/N-156402.html.

Kang B J, Oh J H (2010), "Geometrical characterization of inkjet-printed conductive lines of nanosilver suspensions on a polymer substrate," *Thin Solid Films*, vol. 518, pp. 2890–2896, doi: 10.1016/j.tsf.2009.10.126.

Kang B J, Lee C K, Oh J H (2012), "All-inkjet-printed electrical components and circuit fabrication on a plastic substrate," *Microelectron. Eng.*, vol. 97, pp. 251–254, doi: 10.1016/j.mee.2012.03.032.

Ko S H, Chung J, Hotz N, Nam K H, Girgoropoulos C P (2010), "Metal nanoparticle direct inkjet printing for low-temperature 3D micro metal structure fabrication," *J. Micromech. Microeng.*, vol. 20, 125010, doi: 10.1088/0960-1317/20/12/125010.

Lee D J, Oh J H (2010), "Shapes and morphologies of inkjet-printed nanosilver dots on glass substrates," *Surf. Interf. Anal.*, vol. 42, pp. 1261–1265, doi: 10.1002/sia.3281.

Lee H, Tentzeris M M, Markondeya P, Raj M K P, Kawahara Y (2013), "Inkjet-printed ferromagnetic nanoparticles for miniaturization of flexible printed RF inductors," in *2013 IEEE Antennas and Propagation Society Int. Symp.*, pp. 994–995, doi: 10.1109/APS.2013.6711157.

Li G, Roberts R C, Tien N C (2014), "Interlacing method for micro-patterning silver via inkjet printing," in *2014 IEEE Sensors*, pp. 1687–1690, doi: 10.1109/ICSENS.2014.6985346.

Lim T, Han S, Chung J, Chung J T, Ko S, Grigoropoulos C P (2009a), "Experimental study on spreading and evaporation of inkjet printed pico-liter droplet on a heated substrate," *Int. J. Heat Mass Trans.*, vol. 52, pp. 431–441, doi: 10.1016/j.ijheatmasstransfer.2008.05.028.

Lim T, Jeong J, Chung J, Chung J T (2009b), "Evaporation of inkjet printed pico-liter droplet on heated substrates with different thermal conductivity," *J. Mech. Sci. Technol.*, vol. 23, pp. 1788–1794, doi: 10.1007/s12206-009-0604-0.

Mann J A, Rodríguez-López J, Abruña H D, Dichtel W R (2011), "Multivalent binding motifs for the noncovalent functionalization of graphene," *J. Am. Chem. Soc.*, vol. 133, pp. 17614–17617, doi: 10.1021/ja208239v.

Marjanovic N, Chiolerio A, Kus M, Ozel F, Tilki S, Ivanović. N, Rakočević. Z, Andrić. V, Barudžija T, Baumanna R R (2014), "Magnetite nanoparticles: Synthesis, thin film properties and inkjet printing of magnetic cores for inductor applications," *Thin Solid Films*, vol. 570, pp. 38–44, doi: 10.1016/j.tsf.2014.09.002.

Mei J (2005), "Formulation and processing of novel conductive solution inks in continuous inkjet printing of 3-D electric circuits," *IEEE Trans. Electron. Packag.*, vol. 28, pp. 265–273, doi: 10.1109/TEPM.2005.852542.

Nkosi S S, Kortidis I, Motaung D E, Keartland J, Sideras-Haddadb E, Forbes A, Mwakikunga B W, Kiriakidis G, Sinha-Ray S (2013), "Optical constants correlated electrons-spin of micro doughnuts of Mn-doped ZnO films," *Appl. Surf. Sci.*, vol. 280, pp. 79–88, doi: 10.1016/j.apsusc.2013.04.100.

Shen S C, Pan C T, Wang Y R, Chang C C (2006), "Fabrication of integrated nozzle plates for inkjet print head using microinjection process," *Sensors Actuat. A: Phys.*, vol. 127, pp. 241–247, doi: 10.1016/j.sna.2005.08.016.

Sirringhaus H, Kawase T, Friend R H, Shimoda T, Inbasekaran M, Wu W, Woo E P (2000), "High-resolution inkjet printing of all-polymer transistor circuits," *Science*, vol. 290, pp. 2123–2126, doi: 10.1126/science.290.5499.2123.

Stringer J, Derby B (2009), "Limits to feature size and resolution in inkjet printing," *J. Eur. Ceram. Soc.*, vol. 29, pp. 913–918, doi: 10.1016/j.jeurceramsoc.2008.07.016.

Stringer J, Derby B (2010), "Formation and stability of lines produced by inkjet printing," *Langmuir*, vol. 26, pp. 10365–10372, doi: 10.1021/la101296e.

van den Berg A M J, de Laat A W M, Smith P J, Perelaer J, Schubert U S (2007), "Geometric control of inkjet printed features using a gelating polymer," *J. Mater. Chem.*, vol. 17, pp. 677–683, doi: 10.1039/B612158F.

Wu Y, Rao K V, Voit W, Tamaki T, Jayakumar O D, Belova L, Liu Y S, Glans P A, Chang C L, Guo J H (2010), "Room temperature ferromagnetism and fast ultraviolet photoresponse of inkjet-printed Mn-doped ZnO thin films," *IEEE Trans. Magn.*, vol. 46, pp. 2152–2155, doi: 10.1109/TMAG.2010.2043230.

Wu J, Wang R, Yu H, Li G, Xu K, Tien N C, Roberts R C, Li D (2015), "Inkjet-printed microelectrodes on PDMS as biosensors for functionalized microfluidic systems," *Lab Chip*, vol. 15, pp. 690–695, doi: 10.1039/c4lc01121j.

Yun Y H, Kim J D, Lee B K, Cho Y W, Lee H Y (2009), "Polymer inkjet printing: Construction of three-dimensional structures at micro-scale by repeated lamination," *Macromolecular Res.*, vol. 17, pp. 197–202, doi: 10.1007/BF03218679.

Yung K C, Wu S P, Liem H (2009), "Synthesis of submicron sized silver powder for metal deposition via laser sintered inkjet printing," *J. Mater. Sci.*, vol. 44, pp. 154–159, doi: 10.1007/s10853-008-3119-7.

Yung W K C, Sun B, Huang J, Jin Y, Meng Z, Choy H S, Cai Z, Li G, Ho C L, Yang J, Wong W Y (2016), "Photochemical copper coating on 3D printed thermoplastics," *Sci. Rep.*, vol. 6, 31188, doi: 10.1038/srep31188.